# Interface Phenomena in Magnetron Sputtered Cu$_2$O/ZnO Heterostructures

I.J.T. Jensen,[*,†] S. Gorantla,[‡] O.M. Løvvik,[†] J. Gan,[‡] P.D. Nguyen,[‡] E. Monakhov,[‡] B.G. Svensson,[‡] A.E. Gunnæs,[‡] and S. Diplas[†]

†*SINTEF Materials and Chemistry, P/O box 124 Blindern, 0314 Oslo, Norway*

‡*Department of Physics/Center for Materials Science and Nanotechnology, University of Oslo, P/O box 1048 Blindern, 0316 Oslo, Norway*

E-mail: IngvildThue.Jensen@sintef.no

**Abstract**

The interface between ZnO and $Cu_2O$ has been predicted to be a good candidate for use in thin film solar cells. However, the high predicted conversion efficiency has yet to be fully realized experimentally. To explore the underlying causes of this we investigate the interface between ZnO and $Cu_2O$ in magnetron sputtered samples. Two different sample geometries were made: In the first set thin layers of ZnO were deposited on $Cu_2O$ (type A), while in the second set the order was reversed (type B). Using x-ray photoelectron spectroscopy (XPS), an intermediate CuO layer was identified regardless of the order in which the $Cu_2O$ and ZnO layers were deposited. The presence of a CuO layer was supported by transmission electron microscopy (TEM) results. Changes in the electron hole screening conditions were observed in CuO near the interface with ZnO, manifested as changes in the relative peak-to-satellite ratio and the degree of asymmetric broadness in the Cu 2p peak. The suppression of the Cu 2p satellite characteristic of CuO may cause the CuO presence to be overlooked and cause errors in determinations of valence band offsets (VBOs). For the type A samples, we compare four different approaches to XPS-based determination of VBO and find that the most reliable results are obtained when the thin CuO layer and the altered screening conditions at the interface were taken into account. The VBOs were found to range between 2.5 eV and 2.8 eV. For the B type samples a reduction of the Cu 2p-LMM Auger parameter was found as compared to bulk $Cu_2O$, indicative of quantum confinement in the $Cu_2O$ overlayer.

# Introduction

Metal oxides are an abundant class of materials displaying a wide range of interesting properties, such as superconductivity,[1] colossal magnetoresistance[2] and simultaneous transparency and conductance.[3] Controlling interfaces between oxides at the nano scale has set the stage for phenomena such as 2D electronic gas[4] and magneto-electric coupling,[5] and interfaces are also central in the application of metal oxide semiconductors in optoelectronic devices.

Metal oxide semiconductors have wide bandgaps ($E_g$), which can be used to harvest energy also from the range of the solar spectrum inaccessible for conventional Si solar cells. A complicating factor in this respect is the p/n-type doping asymmetry experienced for metal oxide semiconductors.[6] This means that p-n junctions will have to be made in the form of heterojunctions, which makes optimisation of the interface between different metal oxide semiconductors of crucial importance.

$Cu_2O$ ($E_g = 2.1$ eV) is one of the few p-type metal oxides available.[6] Paired with n-type ZnO ($E_g = 3.4$ eV) it is seen as a promising material for photovoltaic devices, with a theoretical conversion efficiency of about 23%.[7] A variety of deposition techniques have been employed to create the $Cu_2O$/ZnO interface, e.g., magnetron sputtering,[8] pulsed laser deposition,[9] vacuum arc plasma evaporation,[10] atomic layer deposition (ALD),[11] and molecular beam epitaxy,[12] but to date no one has come close to reaching the theoretical conversion efficiency. There seems to be a general consensus that the lack of success is related to difficulties in controlling the interface between $Cu_2O$ and ZnO.[13]

For oxide semiconductors, oxidation processes and interface properties may depend strongly on deposition conditions.[14,15] When exposed to air, a layer of CuO will form on the surface of Cu and $Cu_2O$.[14,16] The formation of CuO on the $Cu_2O$ surface prior to ZnO deposition has been reported to be a limiting factor for the performance of devices based on $Cu_2O$/ZnO heterojunctions.[17] In our recent work, however, transmission electron microscopy (TEM) results showed a thin layer of CuO ($\sim 5$ nm) present at the interface also when $Cu_2O$ was deposited on ZnO substrates.[18] The CuO formation can be linked to relaxation of the strain caused by the lattice mismatch between ZnO and $Cu_2O$. The thin layer of CuO acts as a template for $Cu_2O$ growth and appears to be inherent to the ZnO/$Cu_2O$ interface.[19]

Differentiating between $Cu_2O$ and CuO in layered thin film samples can be challenging. In the present work, we use X-ray photoelectron spectroscopy (XPS) to investigate oxidation processes and the electronic structure/band conditions at the $Cu_2O$/CuO/ZnO interface. $Cu_2O$ and CuO can be distinguished in XPS by differences in their Cu 2p peak position and

shapes. A good overview of the Cu 2p characteristics of Cu metal, oxides and hydroxides can be found in the work of Biesinger *et al.*[20] In addition to being shifted by about 1.2 eV to higher binding energy ($E_B$), the CuO peak is significantly broader and CuO has very characteristic shake-up satellites between 7 and 11 eV from the main peak. $Cu_2O$ has a weaker satellite structure located at higher $E_B$. The satellites and the asymmetric broadness of the Cu 2p main peak in CuO are closely linked to the relaxation of the electronic structure after photoelectron emission.[21] The XPS results are supplemented by density functional theory (DFT) calculations and experimental data from X-ray diffraction (XRD) and transmission electron microscopy (TEM).

## Methods

Two different sets of samples were investigated, as illustrated in figure 1. Thin film samples were first fabricated on quartz substrates (sample set A) using a commercial DC/RF Magnetron Sputter system (Semicore Triaxis). Substrates were treated in consecutive ultra-sonic baths using acetone, isopropanol and deionized water; 10 minutes each. Subsequently, the substrates were dried with a nitrogen flow and loaded into the growth chamber. The targets used were copper and 2 at.% Al doped ZnO (AZO) plates. The base pressure was below $4.4 \times 10^{-4}$ Pa at the substrate temperature of 400 °C, while the total pressure during the deposition was stable after the igniter was turned on. The target-substrate distance was measured to be 7.2 cm with the target surface being parallel to the substrate. Additionally,
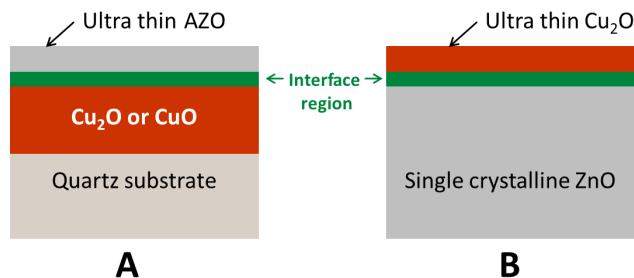


Figure 1: (Color online) Schematic representation of sample set A (left) and B (right).

**Table 1: Processing parameters for the reactive radio frequency sputter deposition.**

| Sample Type | Target | $Q(\mathrm{Ar})$ [a)] [sccm] | $Q(\mathrm{O_2})$ [a)] [sccm] | $P_p$ [b)] [Pa] | $P_T$ [c)] [W] | $t$ [d)] [min] |
|---|---|---|---|---|---|---|
| Quartz/Cu$_2$O | Cu | 20.0 | 3.7 | 0.74 | 250 | 15 |
| Quartz/CuO | Cu | 20.0 | 3.7 | 0.84 | 49 | 100 |
| Quartz/Cu$_2$O/AZO | Cu | 20.0 | 3.7 | 0.77 | 250 | 2 |
| (AZO: 1, 3, 5, 10 nm) | AZO | 70.0 | 0.0 | 2.31 | 49 | (0.5, 1.5, 2.5, 5) |
| Quartz/CuO/AZO | Cu | 19.7 | 3.0 | 0.81 | 49 | 15 |
| (AZO: 1, 3, 5 nm) | AZO | 69.7 | 0.0 | 2.32 | 49 | (0.5, 1.5, 2.5) |
| ZnO/Cu$_2$O | Cu | 19.8 | 3.0 | 0.74 | 205 | $\sim 5$ s |

a) $Q(\mathrm{Ar})$ and $Q(\mathrm{O_2})$ is the argon and oxygen mass flow, respectively.

b) $P_P$ is the plasma pressure during the deposition.

c) $P_T$ is the target power.

d) $t$ is the sputtering time.

the sample stage was rotated at a constant speed of 12 rpm during deposition in order to attain good film uniformity. The deposition rates for Cu$_2$O were $\sim 40$ nm/min for target power $P_\mathrm{T} = 250$ W and $\sim 10$ nm/min for $P_\mathrm{T} = 49$ W. The deposition rate for AZO was $\sim 2$ nm/min. After sputtering, the O$_2$ flow was turned off immediately before closing the target shutter to suppress oxidation of Cu$_2$O, which is sensitive to O$_2$ at elevated temperatures. The thin film layers were deposited in one run, i.e., without breaking vacuum. Four samples were made with increasing thickness $d_\mathrm{AZO}$ of the AZO overlayer, in order to vary the distance from the sample surface to the interface. The nominal thicknesses were $d_\mathrm{AZO} =1$ nm, 3 nm, 5 nm and 10 nm. A clear trend of increasing $d_\mathrm{AZO}$ was observed by XPS, but as discussed later, TEM investigations revealed the Cu$_2$O/AZO interface to be quite rough, leaving the absolute values of $d_\mathrm{AZO}$ uncertain. For this reason the type A samples have been labelled a, b, c, and d, with $d_\mathrm{AZO}$ increasing from a to d. Due to the rough interface observed in the type A samples, a second approach to sample synthesis was employed: In sample set B, Cu$_2$O was sputter deposited directly onto single crystal c-axis oriented ZnO substrates. The substrate wafers were double-side polished and pre-treated as described above for quartz to make sure they were free of any contamination before the sputtering deposition. One side of

such a prepared wafer served as the O-polar substrate while the other side as the Zn-polar substrate. After deposition the films were investigated by XRD using a Bruker AXS D8 Discover instrument with Cu K$\alpha$ X-rays.

The samples were investigated by XPS using two different instruments; Thermo Theta Probe ARXPS and Kratos AXIS Ultra$^{DLD}$, both with monochromatic Al K$\alpha$ radiation ($h\nu = 1486.6$ eV) operated at 15 kV and 15 mA. The latter instrument also has a monochromatic Ag L$\alpha$ source ($h\nu = 2984$ eV), operated at 15 kV and 15 mA. Type A samples were investigated using the Al K$\alpha$ source, while the Ag L$\alpha$ source was used for the type B samples. The step size was 0.1 eV for core- and Auger peaks and 0.05 eV for spectra from the valence band maximum region. The pass energy was 20 eV. For the B type samples with $Cu_2O$ on top, an area of about 2 x 2 mm$^2$ was gently sputtered with an Ar$^+$ beam of 0.5 kV delivering 100 $\mu$A of current for 5 minutes. Sputter tests were performed on $Cu_2O$ and CuO reference samples, confirming the expected tendency of reduction of copper oxides upon sputtering; from CuO towards $Cu_2O$ and from $Cu_2O$ towards Cu.[22] Even with a 10 nm ZnO overlayer it was possible to obtain a weak XPS spectra from the $Cu_2O$ layer using Al K$\alpha$ radiation. We attribute this to the roughness of the $Cu_2O$/ZnO interface, which may cause local variations in the thickness of the overlayer. Since the X-ray spot is several orders of magnitude larger than the variations in interface topography we still expect to pick up on possible trends caused by an increase of the mean overlayer thickness. The spectra were fitted using CasaXPS[23] after Shirley background subtraction.[24]

Cross-section TEM specimens were prepared by the conventional tripod wedge mechanical polishing protocol. The final thinning of the specimens was done by ion-milling for about 3 hr in a Fischione 1010 instrument with gradually decreasing beam energy and current of 5 kV and 5 mA, 1 kV and 3 mA and 0.2 kV and 3 mA and respectively, and milling angle from $\pm 8°$ down to $\pm 6°$ at the final polishing stage on both sides of the specimen. A JEOL 2100F microscope operated at 200 kV and a FEI Titan G2 60-300 microscope equipped with a DCOR probe Cs-aberration corrector, operated at 300 kV, was used in the present study.

Scanning TEM (STEM) high-angle annular dark field (HAADF) Z-contrast imaging was performed using the FEI microscope with a probe current of $\sim$ 80 pA and probe convergence and collection angles of 22 mrad and 76-200 mrad range, respectively. The resulting spatial resolution was $\sim$ 0.08 nm. HAADF images show primarily atomic number (Z) contrast and, in the present case, high resolution (HR) HAADF images offer advantage over HRTEM ones owing to the direct correlation between the image contrast and the cation positions. Fast Fourier Transform (FFT) analysis was used on HR images to identify the different phases of Cu-O in the film.[25,26]

DFT calculations were performed with the Vienna ab-initio simulation package (VASP)[27,28] using the Perdew-Burke-Ernzerhof gradient approximation[29] and the projector augmented wave method.[30] The plane-wave cut-off was 400 eV and the k-point density was at least 4 points per Å$^{-1}$ in each unit cell direction. The force relaxation criterion was 0.05 eV/Å. Details of the structural relaxation can be found elsewhere.[19] Bader analysis[31] was performed to study the charge distribution across the CuO/ZnO interface.

## Results and discussion

### Structure and screening effects at the interface

Figure 2 a) shows a representative XRD diffractogram for the Type A samples, with Bragg reflections from $Cu_2O$ (111), (200) and (311). The lattice parameters agrees with the reported value for $Cu_2O$ within $\pm 0.2\%$.[32] The ZnO overlayer was too thin to be detected, and there is no visible sign of CuO in the diffractograms. Figure 2 b) shows a TEM bright field image from a corresponding sample where the ZnO overlayer has been grown thicker to prevent damage to the $Cu_2O$/ZnO interface during TEM sample preparation. Columnar growth of $Cu_2O$ normal to the substrate, with grain widths of about 100 nm, is observed. The interface between $Cu_2O$ and ZnO is not planar.

From the XPS investigation of sample set A, the copper oxide layer close to the AZO

a)

Cu$_2$O (111)

Cu$_2$O (200)

Cu$_2$O (311)

Intensity [arb. units]

30    40    50    60    70    80

2θ [degree]

b)

Quartz substrate

Cu$_2$O ~640 nm

ZnO ~110 nm

100 nm
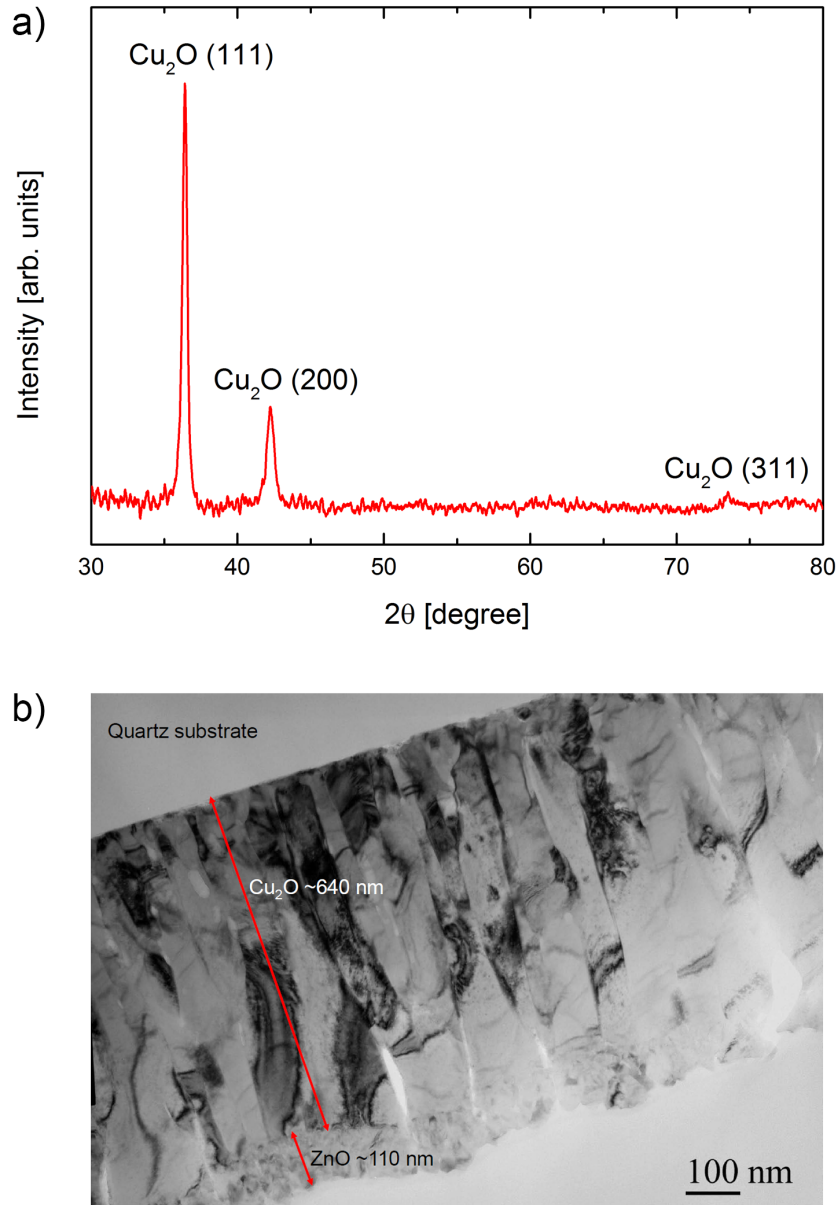
Figure 2: (Color online) a) XRD results from sample type A. b) TEM bright field image from a corresponding sample with thicker ZnO layer on top.

interface was found to resemble CuO more than $Cu_2O$, with the characteristic Cu 2p satellite structure of CuO clearly visible. Figure 3 a) shows the Cu 2p $^3/_2$ peak for the $Cu_2O$/AZO samples a, b and c compared to the CuO reference sample.

The Cu 2p peak looks more like CuO than $Cu_2O$ at the interface with AZO, but the peak appears to be shifted slightly to lower $E_B$ and the full width at half maximum (FWHM) becomes more narrow as the thickness of the AZO layer increases. This could have been an indication that the peak contains contributions from both $Cu_2O$ and CuO, e.g., due to presence of CuO at the $Cu_2O$/ZnO interfaces as a result of oxidation of $Cu_2O$ prior to or during deposition of ZnO. Interestingly, figure 3 also reveals that the peak-to-satellite intensity ratio increases for increasing thickness of the AZO toplayer, i.e., the Cu 2p satellite becomes relatively weaker the closer one gets to the interface with the AZO layer. (Because of the limited escape depth of the photoelectrons an increase in the AZO overlayer thickness effectively means that the Cu 2p signal will come from closer to the ZnO interface.) A control experiment was performed on samples with corresponding AZO films on top of CuO, figure 3 b). The same increase in the peak-to-satellite intensity ratio was found also for the interface in these samples, suggesting that the phenomenon is related to the interaction between copper and zinc oxide at the interface, rather than being caused by a mixture of $Cu_2O$ and CuO within the XPS sampling volume.

The creation of the core hole upon photoelectron emission triggers intra- and extra-atomic relaxation phenomena, e.g., screening which take place via charge re-distribution inside the photoionised atom or by charge transfer from the surrounding atoms to the ionised atom, respectively. These processes are final state effects and can lead to additional peaks at the high binding energy side of the main photoelectron peak, labelled "shake up satellites". The phenomenon can be understood as a result of the excitation (shake-up), by the emitted photoelectron, of an electron from the valence to the conduction band with a concomitant loss in the kinetic energy of the photoelectron. For CuO it has been shown that the most energetically favourable final state, i.e., the main Cu 2p peak, is produced by non-local

9

screening from surrounding Cu atoms ($2\underline{p}\,3d^{10}$, where $2\underline{p}$ denotes a hole in the 2p orbital). Local screening from the ligand O atom produce final states at slightly higher energies ($2\underline{p}\,3d^{10}\,\underline{L}$, where $\underline{L}$ denotes a hole in the valence band of the ligand), which give raise to the asymmetric broadening of the Cu 2p main peak in CuO. The satellite, on the other hand, is mainly a result of poorly screened states ($2\underline{p}\,3d^{9}$).[21,33]
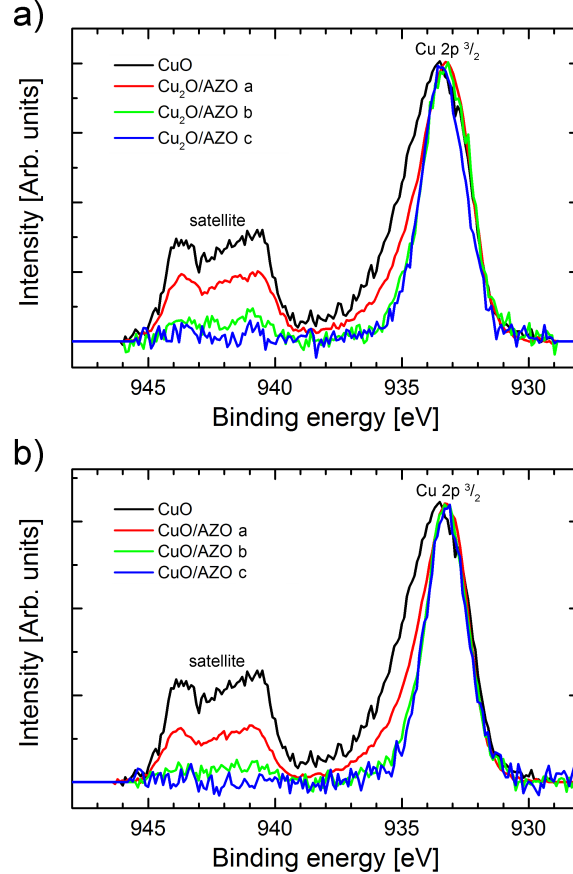


Figure 3: (Color online) Cu 2p XPS spectra from type A samples a (red), b (green) and c (blue) with AZO toplayer on $Cu_2O$ (top) and CuO (bottom); compared to the CuO reference sample (black).

It has been shown that different types of next nearest neighbor metal ions may influence the final states after photoemission:[34] The shake-up satellite to main peak intensity ratios and FWHM of metal 2p levels for $Co^{2+}$ and $Cu^{2+}$ in MgO were found to be smaller than those for CoO and CuO. In $Cu_xMg_{1-x}O$ compounds the satellite intensity was found to decrease with decreasing $x$. Mg is significantly less electronegative than both Co and Cu, potentially
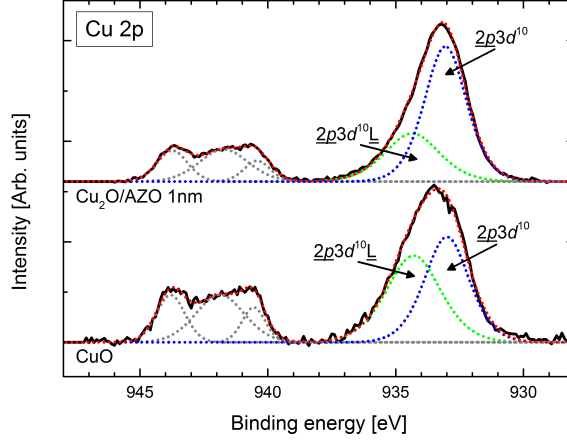
Figure 4: (Color online) Fitting of Cu 2p $^3/_2$ peak with to components corresponding to non-local ($\underline{2p}\,3d^{10}$) and local ($\underline{2p}\,3d^{10}\,\underline{L}$) screening. Different intensity ratios of the two components result in variations in the asymmetric broadness of the convoluted peak.

leading to better screening of the Co and Cu 2p core holes. Also for $CuF_2$, $CuCl_2$ and $CuBr_2$ the satellite intensity was found to decrease with decreasing electronegativity of the neighboring cation. Thus the reduced satellite intensity observed in the Cu 2p spectra close to the CuO/ZnO interface could be due to improved screening resulting from the proximity to Zn atoms, which are less electronegative than Cu (Pauling electronegativity 1.65 and 1.90, respectively).

For the $Cu_2O$/AZO and CuO/AZO (type A) samples the Cu 2p $^3/_2$ peak could be fitted with two components corresponding to the two alternative final states $\underline{2p}\,3d^{10}$ and $\underline{2p}\,3d^{10}\,\underline{L}$, as illustrated in Figure 4. Thus the decrease in asymmetric broadening observed in figure 3 can be understood as a change in the relative intensity of the $\underline{2p}\,3d^{10}$ and $\underline{2p}\,3d^{10}\,\underline{L}$ components. At the interface Cu will share ligands with Zn, which may change the screening conditions. In order to investigate this, Bader analysis was performed on a CuO/ZnO interface model produced by DFT. Figure 5 shows the DFT-model. The calculated average valence charge per atom was found to be 9.9 e for Cu and 10.7 e for Zn, compared to 11 e and 12 e in the respective elemental states. For O the calculated average valence charge per atom was found to be 7.2 e on the ZnO side and 7.0 e on the CuO side, compared to 6 e in the elemental state. No significant variations were found as a function of distance to the

11

interface. The O atoms at the interface, which have bonds with both Zn and Cu, were found to behave the same as O atoms in the middle of the CuO layer. Thus, we conclude that the change in asymmetric peak broadness observed for Cu 2p is caused by changes in the non-local screening conditions, rather than the local screening by the ligand. As Zn is less electronegative and has an extra electron compared to Cu, it makes sense that introducing Zn in the neighbourhood will cause increased intensity for the $\underline{2p}\,3d^{10}$ component (the well screened state).
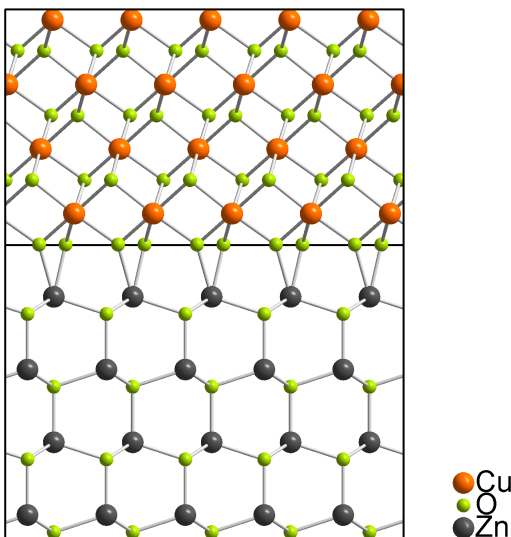


Figure 5: (Color online) The DFT interface model used for the Bader analyis: CuO (above interface) and ZnO (below interface). Small balls represent O and large balls represent Cu (top) or Zn (bottom).

In order to improve the smoothness of the $ZnO/Cu_2O$ interface, $Cu_2O$ was deposited on single crystalline ZnO, both O- and Zn-face (type B samples). Due to technical limitations in the sputtering deposition setup, it was not possible to grow a $Cu_2O$ overlayer that was sufficiently thin to allow detection of the ZnO underneath. Thus a gentle $Ar^+$ sputtering was employed in order to detect Zn 2p photoelectrons. Figure 6 shows Cu and Zn 2p spectra before and after $Ar^+$ sputtering. Before sputtering, the Cu 2p signal had the distinct characteristics of $Cu_2O$, while no clear peaks were seen in the Zn 2p region. After 5 minutes of sputtering, the Zn 2p peaks appear and the Cu 2p spectrum displays the characteristics of CuO. We feel certain that the changes in the Cu 2p peak were not induced by the $Ar^+$

sputtering, as this should have caused a reduction in the O:Cu ratio rather than an increase.[22]
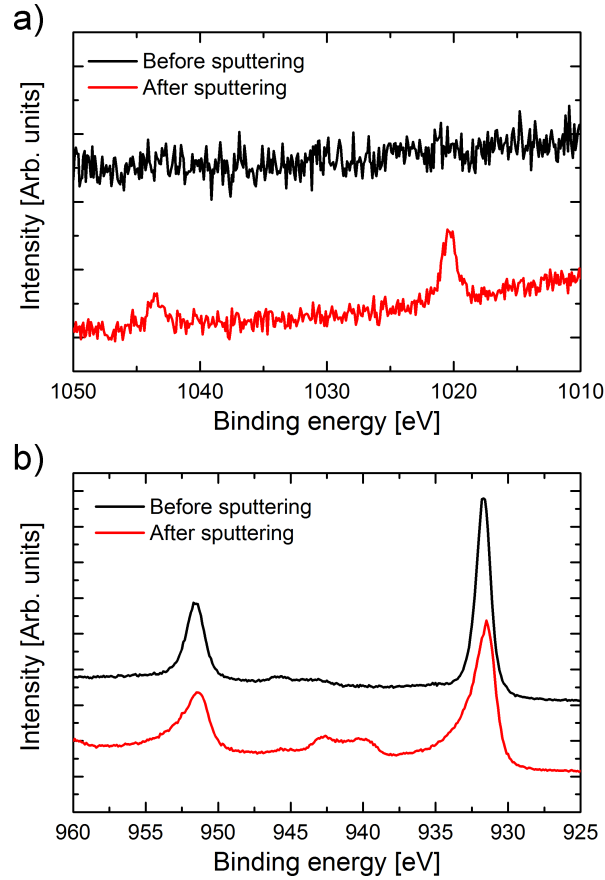


Figure 6: (Color online) Zn 2p (a) and Cu 2p (b) spectra from $Cu_2O$ on single crystalline ZnO (Zn-face), before (top) and after (bottom) gentle $Ar^+$ sputtering. The same results were obtained for $Cu_2O$ deposited on O-face single crystalline ZnO.

One of the samples with a 5 nm thick $Cu_2O$ film deposited on single crystal ZnO was further investigated by high-resolution scanning transmission electron microscopy dark field imaging (STEM HAADF). As shown in figure 7, we clearly observe the presence of few atomic layers thick ($\sim 1.5$ nm) CuO grains at the interlayer between ZnO and $Cu_2O$. The fast fourier transforms from the grains immediately above the ZnO substrate match with the CuO phase, as shown in figure 7 (c) and grains further away from ZnO match with $Cu_2O$, as shown in figure 7 (b). We have consistently observed this trend at different areas of the cross-section STEM sample. The grains of CuO were observed to have discrete random orientations that allow their planes with hexagonal ionic arrangement to be parallel with

ZnO (0001) surface, e.g., $(111)[1\bar{1}0]_{Cu_2O} \parallel (1\bar{1}\bar{1})[01\bar{1}]_{CuO} \parallel (0001)[11\bar{2}0]_{ZnO}$, as is the case in figure 7 (a). This is consistent with our previous observations of the presence of a CuO interlayer on relatively thick $Cu_2O$ films deposited on single crystal ZnO bulk samples.[19]
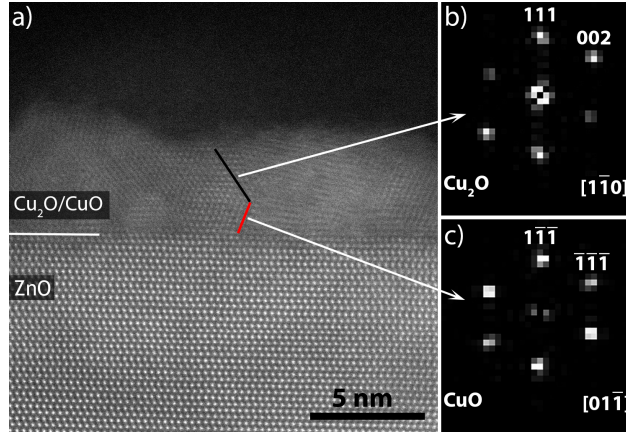


Figure 7: (Color online)(a) High-resolution scanning transmission electron microscopy dark field (HAADF) image of the cross-section of the sample used for XPS measurement where $\sim 5$ nm thick $Cu_2O$ film was deposited on ZnO substrate. In the film, the difference in the orientation and interatomic spacing of the lattice planes to the left of black and red lines clearly show the presence of two different phases of Cu-O. The corresponding FFTs from the region in film to the left of black and red lines, are shown in (b) and (c), match with $Cu_2O$ and CuO phases respectively.

As mentioned previously, a layer of CuO will tend to form on $Cu_2O$ surfaces under ambient conditions. CuO is known to be detrimental for electronic properties of the Cu2O/ZnO interface, e.g., for samples grown by atmospheric ALD, CuO formation on $Cu_2O$ before and during deposition of ZnO has been shown to reduce the open circuit voltage of the $Cu_2O$/ZnO heterojunction.[17] The CuO-like interface layer seen in our A samples (Fig. 3) is consistent with formation of CuO on $Cu_2O$ during switching to ZnO growth. However, the CuO-like interface layer was also seen in our B samples, where $Cu_2O$ was deposited on single crystalline ZnO (Fig. 6). Thus, regardless of the order of deposition/growth, a CuO-like intermediate layer tends to form between ZnO and $Cu_2O$. The driving force for the formation of CuO phase is most likely to minimize the lattice misfit interfacial strain between $Cu_2O$ and ZnO.[19]

## Auger parameters

In order to further analyse the XPS data, we employ the concept of Wagner plots.[35] The absolute position of the peaks from both ZnO and Cu$_2$O may be affected both by interface band bending and sample charging, which makes it difficult to find a good common reference point to use in the comparison between Cu$_2$O samples with AZO toplayer and the Cu$_2$O and CuO reference samples. The commonly employed practice of using the C 1s signal from adventitious carbon for binding energy referencing can be misleading.[36] However, using the final state Auger parameter (AP) both band bending and sample charging are effectively cancelled out. The final state Auger parameter is given as:

$$\alpha\prime = E_{\mathrm{K}}(\text{Auger peak}) + E_{\mathrm{B}}(\text{Core peak}) \qquad (1)$$

where $E_{\mathrm{K}}(\text{Auger peak})$ is the kinetic energy associated with an Auger electron and $E_{\mathrm{B}}(\text{Core peak})$ is the binding energy of a corresponding core photoelectron. The Wagner plot is a fruitful way to present information on both absolute peak positions and Auger parameters, which makes it possible to distinguish between actual changes in chemical state and shifts due to band bending, sample charging etc. For thin film samples, however, it is important to pay attention to the difference in sampling depth of the peaks to be compared. Figure 8 shows what we have chosen to label *apparent* Wagner plots for Zn and Cu, since the difference in sampling depth between the core and Auger peaks is on a scale comparable to the thickness of the layers in our samples.[37] For Zn in figure 8 a) the $\alpha\prime$ is constant (within the accuracy of 0.15 eV) and what appears to be an overall upward band bending (photoelectron peak moves towards the Fermi level) can be seen as the thickness of the AZO toplayer decreases. For the ZnO in the CuO/AZO b and c samples, on the other hand, there seems to be downward band bending compared to the reference samples. We think this is highly unlikely and take it as an indication of sample charging, which seems consistent also with the Cu data. For Cu$_2$O/AZO the Zn 2p-LMM AP is $2010.0 \pm 0.15$ eV, compared to $2010.1 \pm 0.15$ eV for

CuO/AZO and the AZO reference samples.
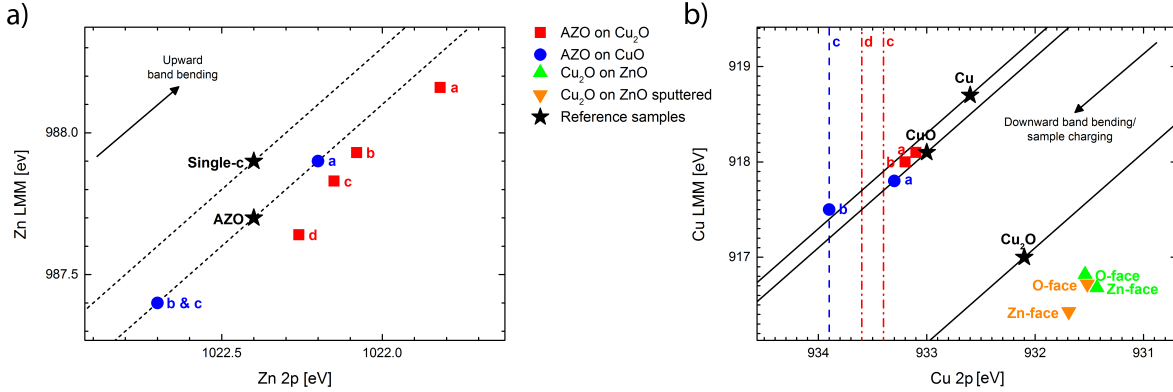


Figure 8: (Color online) *Apparent* Wagner plots for Zn (a) and Cu (b). The Auger parameter of the reference samples are shown as lines with slope -1. The vertical lines mark Cu 2p positions in the samples where the corresponding Cu LMM peak was too weak to be measured.

Figure 8 b) shows the corresponding results for Cu. For the thickest AZO overlayers the Cu 2p positions are shown as vertical lines, as the corresponding Auger peaks were too weak for the AP to be determined. For the type A samples the position of the main component of the Cu 2p $^3/_2$ and Cu LMM spectra correspond closely to the AP of the CuO reference sample at 1851.1 eV. This is lower than the commonly reported AP of CuO at 1851.33 eV[20] since the two different screening states are not usually resolved in routine fittings of the Cu 2p $^3/_2$ peak. When fitting the Cu 2p $^3/_2$ peak of our CuO referance sample with only one (asymmetric) component the AP becomes 1851.3 eV. A shift towards lower $E_B$ with increasing thickness of the AZO layer can be seen for all the type A samples, indicative of sample charging and/or downward bandbending. The distance between the Zn 2p and the Cu 2p peak positions is however found to be practically identical for the different samples. This suggests that either the change of band bending is exactly the same for both Zn and Cu or that the shifts observed for the A type samples (figure 8) are caused by sample charging. Although the latter is clearly the most probable solution, it does not explain why the Zn peaks in the $Cu_2O$/AZO samples shift to *lower* $E_B$ compared to the AZO reference sample. Comparing the C 1s peak positions of adventitious carbon in the different samples does

not solve the problem. It could be that the position of the Fermi level within the bandgap was slightly shifted in the AZO reference sample compared to the layered samples (due to different defects like Cu-related acceptors).

For the ZnO/Cu$_2$O (type B) samples, both the absolute peak positions and AP are markedly different from both the Cu$_2$O and CuO reference samples. As the XPS sampling volume in the B type samples consists primarily of Cu$_2$O on top of the CuO-like interface layer, one would expect AP to be close to the value for pure Cu$_2$O; $\alpha\prime = 1849.2$ eV, perhaps with a shift towards the higher AP of pure CuO. Instead we find an AP which is about 1 eV *lower* than pure Cu$_2$O, which can not be explained just by assuming a mixture of Cu$_2$O and CuO contribution to the spectra. Previously, an apparent *"asymmetry"* in band alignment across Cu$_2$O/ZnO and ZnO/Cu$_2$O interfaces has been related to estimated differences in lattice distortion,[38] while decrease of the AP as function of size/thickness (and substrate) has been reported for deposition of Cu$_2$O on ZrO$_2$ and SiO$_2$.[39] In view of reports of an intense quantum confinement effect in Cu$_2$O thin films,[40] and our observed *"symmetry"* in formation of a CuO-like interface layer, it is reasonable to interpret the decrease in AP as an effect primarily caused by the Cu$_2$O film thickness, rather than the interface with ZnO. In a simplified view, quantum confinement can be described using the particle-in-a-box concept, in which the separation between energy levels is increased. Increased separation between levels leads to decrease in AP, which is consistent with the experimental data. Thus, it appears that XPS measurements of band offsets across interfaces with thin Cu$_2$O layers on top of ZnO will not be representative for devices based on thicker Cu$_2$O layers.

## Band bending and valence band offsets

When it comes to measuring the valence band maxima and offsets (VBM and VBO, respectively) for our Cu$_2$O/AZO samples, the standard XPS approach is to use two reference

samples (ref) and an interface sample (int):[41]

$$\text{VBM}^{\text{int}} = \text{E}^{\text{int}}_{\text{Core peak}} - [\text{E}^{\text{ref}}_{\text{Core peak}} - \text{VBM}^{\text{ref}}] \tag{2}$$

$$\text{VBO}^{\text{int}} = \text{VBM}^{\text{int}}_{\text{CuO}} - \text{VBM}^{\text{int}}_{\text{ZnO}} \tag{3}$$

where $\text{E}_{\text{Core peak}}$ is the position of the Cu and Zn 2p peaks in this work (using Zn 3p gave the same result as Zn 2p). Since eq. 3 only contains relative distances between peaks in each spectrum, potential problems related to sample charging are cancelled out. The method does however require detailed knowledge of the structure at the interface, in order to select the appropriate reference samples. In the $Cu_2O/ZnO$ samples, for instance, larger scale characterisation methods, such as X-ray diffraction, does not detect the thin layer of CuO which is present at the interface.[18] Figure 9 a) shows a schematic representation of the band structure across a CuO/ZnO interface, with a red oval marking the valence band offset at the interface ($\text{VBO}^{\text{int}}$). In table 2, we have calculated the $\text{VBO}^{\text{int}}$ using both $Cu_2O$ and CuO samples as the reference in eq. 2 (Method $i$ and $ii$, respectively). For CuO we also show two different fitting approaches for the main Cu 2p peak: one where the two alternative final states $\underline{2p}\,3d^{10}$ and $\underline{2p}\,3d^{10}\,\underline{\text{L}}$ are resolved (using the peak position of $\underline{2p}\,3d^{10}$ in the VBO calculation) and one where the peak is just fitted with one asymmetric component (Method $ii(2)$ and $ii(1)$, respectively). As can be seen from the results in table 2, using CuO and $Cu_2O$ leads to radically different results and even the choice of fitting approaches for CuO seems to play a role. Since AZO is strongly n-type and the copper oxides are p-type, it is also possible to measure the $\text{VBM}^{\text{int}}_{\text{CuO}}$ directly (Method $iii$) using the valence spectra from the interface samples, see figure 9 b). This direct method has the advantage of not being dependent of reference samples, which is useful when dealing with inhomogeneous samples. For all the methods the VBM of AZO was determined using the standard method with an AZO reference sample. As shown in table 2, the direct method and the standard method using CuO fitted with two components give the same result within the error for all samples except CuO/AZO

c. It is to be expected that the accuracy decreases as the AZO layer becomes thicker and the signal from Cu becomes weaker as a consequence. The correspondence between the VBO based on direct measurement of the $\mathrm{VBM}^{\mathrm{int}}_{\mathrm{CuO}}$ and the standard method using CuO fitted with two components strengthens the view that the VBO values obtained using the CuO reference sample and a two component fitting of the Cu 2p $^3/_2$ peak is valid. The VBO does not appear to change significantly between the samples; ranging from 2.5 to 2.8 eV without any clear dependence on AZO layer thickness.
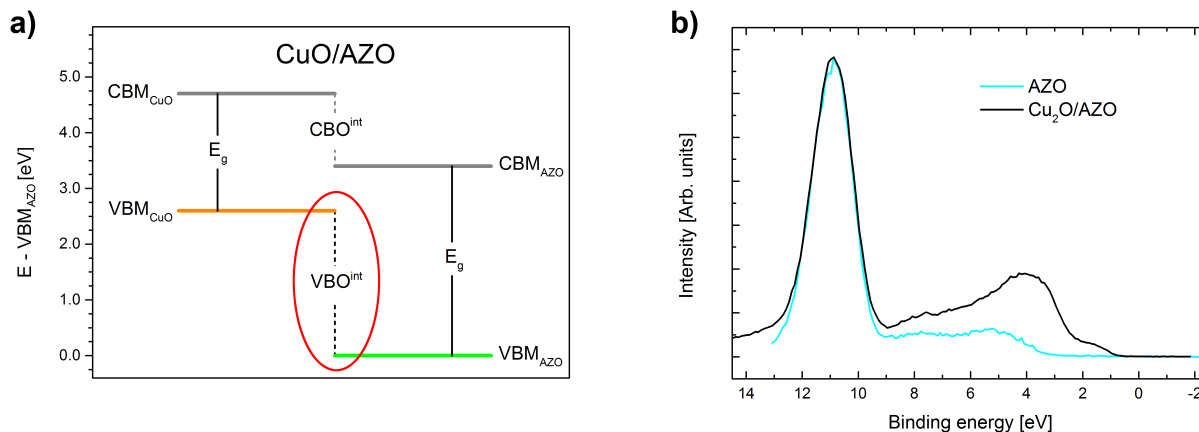


Figure 9: (Color online) a) Schematic band diagram for a CuO/AZO sample. The valence band maxima (VBM) of CuO and AZO were measured using XPS. The red oval marks the valence band offset at the interface (VBO$^{\mathrm{int}}$), corresponding to the values listed in table 2. The conduction band offset at the interface (CBO$^{\mathrm{int}}$)was deduced from the bandgaps (E$_g$) of CuO and AZO. b) Valence spectra from the Cu$_2$O/AZO sample with the thinnest AZO overlayer and the AZO reference sample. The spectra are aligned using the Zn 3p peak to fascilitate visual comparison.

In the literature, VBOs ranging from 1.7 eV to 2.8 eV can be found for heterojunctions based on Cu$_2$O and ZnO, from XPS measurements of samples with different geometries and doping.[42-47] The wide range is not surprising. As described above, the most frequently used method for XPS determination of the VBO across an interface relies on comparison to reference samples. This in term requires a detailed knowledge of the micro (nano) structure at the interface in order to chose the appropriate reference samples. As illustrated in our work, this poses a particular problem for inhomogeneous samples. In a previous section, we showed how the characteristic satellite structure in the Cu 2p spectrum of CuO is subdued as

the distance to the interface with ZnO decreases. This means that for thick ZnO overlayers a spectrum from CuO may easily be mistaken for $Cu_2O$; with large consequences for the calculation of the VBO. Even setting measurement errors aside, the very nature of semi-conductor doping implies large variations of the position of the Fermi level relative to the band edges (up to several eV in wide bandgap semi-conductors).[48] This will in turn give different starting points for the band alignment across interfaces in heterostructures. Defects also influence the distance between the Fermi level and the band edges, e.g., even in undoped ZnO variations in intrinsic defects and common impurities, such as Li, can cause variations and Fermi level pinning, depending on the sample treatment.[49] Thus a certain variation in reported VBOs for the $Cu_2O/ZnO$ system is indeed expected. In the context of device development, it seems evident that each specific sample type must be explicitly characterized in order to obtain the correct properties, simply because the VBO depends strongly on the conditions at the interface.

**Table 2: Valence band offsets measured from XPS spectra using different approaches, as described in the text. The VBM-to-$E_{Core\ peak}$ distances found for the reference samples were 1019.1 eV for AZO, 932.9 eV and 933.1 eV for CuO (method *i* and *ii*, respectively) and 932.1 eV for $Cu_2O$, with measurment error $\pm0.14$ eV.**

| Sample | | Valence Band Offset [eV] ($\pm0.24$ eV) | | | |
|---|---|---|---|---|---|
| Type | AZO layer | Method *i*: $Cu_2O$ ref | Method *ii*(1): CuO ref | Method *ii*(2): CuO ref | Method *iii*: Direct |
| $Cu_2O$/AZO | a | 1.7 | 2.7 | 2.5 | 2.4 |
| | b | 2.0 | 3.1 | 2.8 | 2.7 |
| | c | 1.8 | 2.9 | 2.6 | 2.6 |
| | d | 1.7 | 2.8 | 2.5 | 2.6 |
| CuO/AZO | a | 1.9 | 2.9 | 2.7 | 2.6 |
| | b | 1.8 | 2.9 | 2.6 | 2.8 |
| | c | 1.8 | 2.9 | 2.6 | 3.0 |

# Conclusions

A thin CuO layer was observed at the interface both in samples where Al doped ZnO (AZO) was deposited on top of $Cu_2O$ (sample type A) and samples where $Cu_2O$ was deposited on top of single crystalline ZnO (sample type B). Using XPS we have found differences between the Cu 2p spectra from this CuO layer and the bulk CuO reference sample: The peak-to-satellite intensity ratio was higher in the interface samples, and the Cu 2p $^2/_3$ peek exhibited less asymmetric broadening. This could be explained by changes in the screening conditions near the interface, particularly by the introduction of the more electron rich Zn atoms to the vicinity of Cu (contributing to the non-local screening). The Cu 2p-LMM Auger parameter (AP) at the interface in sample type A was found to correspond well with CuO, the Cu 2p-LMM AP for sample type B was significantly lower than that of both CuO and $Cu_2O$. We suggest that the decrease in AP value is due to quantum confinement, which has been reported for $Cu_2O$ thin films. This means that in terms of electronic structure, e.g., band offsets, XPS samples of type B may not be representative for devices based on thicker layers of $Cu_2O$.

The relative valence band maxima (VBMs) of CuO in the type A samples were obtained using four different approaches, see table 2. The most reliable determination of valence band offsets (VBOs) in the $Cu_2O$/ZnO heterostructure was obtained when the thin CuO layer and the altered screening conditions at the interface were taken into account. The VBO appears to rely strongly on the conditions at the interface, and the results emphasize the importance of detailed characterisation of each specific sample type in order to obtain the correct VBO values for heterojunctions intended for device applications.

# Acknowledgements

# References

(1) Bednorz, J. G.; Müller, K. A. Possible high $T_C$ superconductivity in the Ba-La-Cu-O system. *Z. Phys. B - Condensed Matter* **1986**, *64*, 189–193.

(2) Jin, S.; Tiefel, T. H.; McCormack, M.; Fastnacht, R. A.; Ramesh, R.; Chen, L. H. Thousandfold Change in Resistivity in Magnetoresistive La-Ca-Mn-O Films. *Science* **1994**, *264*, 413–415.

(3) Ginley, D. S., Bright, C., Eds. *Special issue on transparent conductive oxides*; MRS Bull., 2000; Vol. 25.

(4) Ohtomo, A.; Muller, D. A.; Grazul, J. L.; Hwang, H. Y. Artificial charge-modulation in atomic-scale perovskite titanate superlattices. *Nature* **2002**, *419*, 378–380.

(5) Ramesh, R.; Spaldin, N. A. Multiferroics: progress and prospects in thin films. *Nature Mater.* **2007**, *6*, 21–29.

(6) Yu, X.; Marks, T. J.; Facchetti, A. Metal oxides for optoelectronic applications. *Nature Mater.* **2016**, *15*, 383–396.

(7) Rühle, S.; Anderson, A. Y.; Barad, H.-N.; Kupfer, B.; Bouhadana, Y.; Rosh-Hodesh, E.; Zaban, A. All-oxide photovoltaics. *J. Phys. Chem. Lett.* **2012**, *3*, 3755–3764.

(8) Gan, J.; Venkatachalapathy, V.; Svensson, B. G.; Monakhov, E. V. Influence of target power on properties of $Cu_xO$ thin films prepared by reactive radio frequency magnetron sputtering. *Thin Solid Films* **2015**, *594*, 250–255.

(9) Nishi, Y.; Miyata, T.; Minami, T. The impact of heterojunction formation temperature on obtainable conversion efficiency in n-ZnO/p-$Cu_2O$ solar cells. *Thin Solid Films* **2013**, *528*, 72–76.

(10) Minami, T.; Miyata, T.; Ihara, K.; Minamino, Y.; Tsukada, S. Effect of ZnO film deposition methods on the photovoltaic properties of ZnO?Cu$_2$O heterojunction devices. *Thin Solid Films* **2006**, *494*, 47–52.

(11) Lee, S. W.; Lee, Y. S.; Heo, J.; Siah, S. C.; Chua, D.; Brandt, R. E.; Kim, S. B.; Mailoa, J. P.; Buonassisi, T.; Gordon, R. G. Improved Cu$_2$O-based solar cells using atomic layer deposition to control the Cu oxidation state at the p-n junction. *Adv. Energ. Mater.* **2014**, *4*, xx.

(12) Darvish, D. S.; Atwater, H. A. Epitaxial growth of Cu$_2$O and ZnO/Cu$_2$O thin films on MgO by plasma-assisted molecular beam epitaxy. *J. Cryst. Growth* **2011**, *319*, 39–43.

(13) Hoye, R. L. Z.; Brandt, R. E.; Ievskaya, Y.; Heffernan, S.; Musselman, K. P.; Buonassisi, T.; MacManus-Driscoll, J. L. Perspective: Maintaining surface-phase purity is key to efficient open air fabricated cuprous oxide solar cells. *Appl. Phys. Mater.* **2015**, *3*, 020901.

(14) Iijima, J.; Lim, J. W.; Hong, S. H.; Suzuki, S.; Mimura, K.; Isshiki, M. Native oxidation of ultra high purity Cu bulk and thin films. *Appl. Surf. Sci.* **2006**, *253*, 2825–2829.

(15) Sumets, M.; Ievlev, V.; Kosteyuchenko, A.; Vakhtel, V.; Kannykin, S.; Kobzev, A. Electrical properties of Si?LiNbO$_3$ heterostructures grown by radio-frequency magnetron sputtering in an Ar + O$_2$ environment. *Thin Solid Films* **2014**, *552*, 32–38.

(16) Lim, J. W.; Iijima, J.; Zhu, Y.; H., Y. J.; Choi, G. S.; Mimura, K.; Isshiki, M. Nanoscale investigation of long-term native oxidation of Cu films. *Thin Solid Films* **2008**, *516*, 4040–4046.

(17) Ievskaya, Y.; Hoye, R. L. Z.; Sadhanala, A.; Musselman, K. P.; MacManus-Driscoll, J. L. Fabrication of ZnO/Cu$_2$O heterojunctions in atmospheric conditions: Improved interface quality and solar cell performance. *Sol. Energ. Mat. Sol. C.* **2015**, *135*, 43–48.

(18) Gan, J.; Gorantla, S.; Riise, H. N.; Fjellvåg, . S.; Diplas, S.; Løvvik, O. M.; Svensson, B. G.; Monakhov, E. V.; Gunnæs, A. E. Structural properties of $Cu_2O$ epitaxial films grown on c-axis single crystal ZnO by magnetron sputtering. *Appl. Phys. Lett.* **2016**, *108*, 152110.

(19) Gunnæa, A. E.; Gorantla, S.; Løvvik, O. M.; Gan, J.; Carvalho, P. A.; Svensson, B. G.; Monakhov, E. V.; Bergum, K.; Jensen, I. J. T.; Diplas, S. Epitaxial strain induced growth of CuO at $Cu_2O$/ZnO interfaces. *J. Phys. Chem. C* **2016**, *41*, 23552–23558.

(20) Biesinger, M. C.; Lau, L. W. M.; Gerson, A. R.; Smart, R. S. C. Resolving surface chemical states in XPS analysis of first row transition metals, oxides and hydroxides: Sc, Ti, V, Cu and Zn. *Appl. Surf. Sci.* **2010**, *257*, 887–898.

(21) van Veenendaal, M.; Sawatzky, G. A. *Phys. Rev. Lett.* **1993**, *70*, 2459.

(22) Panzner, B., G. Egert; Schmidt, H. P. The stability of CuO and $Cu_2O$ surfaces during argon sputtering studied by XPS and AES. *Surf. Sci.* **1986**, *151*, 400–408.

(23) http://www.casaXPS.com. 2012.

(24) Shirley, D. A. High-Resolution X-Ray Photoemission Spectrum of the Valence Bands of Gold. *Phys. Rev. b* **1972**, *5*, 4709–4714.

(25) Suzuki, T. X-Ray Study on the Binding Properties of $Cu_2O$ and $Ag_2O$ Crystals. *J. Phys. Soc. Jpn.* **1960**, *15*, 2018–2024.

(26) Åsbrink, S.; Waɭskowska, A. X-ray Single-Crystal Structure Determination at 196 K and Room Temperature. *J. Phys.: Condens. Matter* **1991**, *3*.

(27) Kresse, G.; Furthmüller, J. Efficient iterative schemes for ab initio total-energy calculations using a plane-wave basis set. *Phys. Rev. B* **1996**, *54*, 11169–11186.

(28) Kresse, G.; Furthmüller, J. Efficiency of ab-initio total energy calculations for metals and semiconductors using a plane-wave basis set. *Comp Mater Sci* **1996**, *6*, 15–50.

(29) Perdew, J. P.; Burke, K.; Ernzerhof, M. Generalized gradient approximation made simple. *Phys. Rev. Lett.* **1996**, *77*, 3865–3868.

(30) Blöchl, P. E. Projector Augmented-Wave Method. *Phys. Rev. B* **1994**, *50*, 17953–17979.

(31) Henkelman, G.; Arnaldsson, A.; Jónsson, H. A fast and robust algorithm for Bader decomposition of charge density. *Comput. Mater. Sci.* **2006**, *36*, 254–360.

(32) Kirfel, A.; Eichhorn, K. D. Accurate structure analysis with synchrotron radiation. The electron density in $Al_2O_3$ and $Cu_2O$. *Acta Crystall. A* **1990**, *46*, 271–284.

(33) Böske, T.; Maiti, K.; Knauff, O.; Ruck, K.; Golden, M. S.; Krabbes, G.; Fink, J. *Phys. Rev. B* **1998**, *57*, 138–141.

(34) Oku, M.; Hirokawa, K. *J. Elec. Spec. Related Phenom.* **1977**,

(35) Moretti, G. Auger parameter and Wagner plot in the characterization of chemical states by X-ray photoelectron spectroscopy: a review. *J. Electron Spectrosc. Relat. Phenom.* **1998**, *95*, 95–144.

(36) Castle, J. E.; Salvi, A. M.; Guascito, M. R. Substrate-related features in the loss structure of contamination C 1s. *Surf. Interface Anal.* **1999**, *27*, 753–760.

(37) Tanuma, S.; Powell, C. J.; Penn, D. R. Calculations of electron inelastic mean free paths. V. Data for 14 organic compounds over the 50?2000 eV range. *Surf. Interf. Anal.* **1994**, *21*, 165–176.

(38) Yang, M.; Zhu, L.; Li, Y.; Cao, L.; Guo, Y. Asymmetric interface band alignments of $Cu_2O/ZnO$ and $ZnO/Cu_2O$ heterojunctions. *J. Alloys Compd.* **2013**, *578*, 143–147.

(39) Espinós, J. P.; Morales, J.; Barranco, A.; Caballero, A.; Holgado, J. P.; González-Elipe, A. R. Interface Effects for Cu, CuO, and $Cu_2O$ Deposited on $SiO_2$ and $ZrO_2$. XPS Determination of the Valence State of Copper in $Cu/SiO_2$ and $Cu/ZrO_2$ Catalysts. *J. Phys. Chem. B* **2002**, *106*, 6921–6929.

(40) Poulopoulos, P.; Baskoutas, S.; Pappas, S. D.; Garoufalis, C. S.; Droulias, S. A.; Za-
mani, A.; Kapaklis, V. Intense Quantum Confinement Effects in $Cu_2O$ Thin Films. *J.
Phys. Chem. C.* **2011**, *115*, 14839–14843.

(41) Kraut, E. A.; Grant, R. W.; Waldrop, J. R.; Kowalczyk, S. P. Precise determination of
the valence-band edge in X-Ray photoemission spectra: Application to measurement
of semiconductor interface potentials. *Phys. rev. Lett* **1980**, *44*, 1620–1623.

(42) Wilson, S.; Bosco, J. P.; Tolstova, Y.; Scanlon, D. O.; Watson, G. W.; Awater, H. A.
Interface stoichiometry control to improve device voltage and modify band alignment
in $ZnO/Cu_2O$ heterojunction solar cells. *Energy Environ. Sci.* **2014**, *7*, 3606.

(43) Ichimura, M.; Song, Y. Band Alignment at the $Cu_2O/ZnO$ Heterojunction. *Jpn. J.
Appl. Phys.* **2011**, *50*, 051002.

(44) Wong, L. M.; Chiam, S. Y.; Huang, J. Q.; Wang, S. J.; Pan, J. S.; Chim, W. K. Growth
of $Cu_2O$ on Ga-doped ZnO and their interface energy alignment for thin film solar cells.
*J. Appl. Phys.* **2010**, *108*, 033702.

(45) Ozawa, K.; Oba, Y.; Edamoto, K. Formation and characterization of the Cu2O overlayer
on Zn-terminated ZnO(0 0 0 1). *Surf. Sci.* **2009**, *603*, 2163–2170.

(46) Kramm, B.; Laufer, A.; Reppin, D.; Kronenberger, A.; Hering, P.; Polity, A.;
Meyer, B. K. The band alignment of $Cu_2O/ZnO$ and $Cu_2O/GaN$ heterostructures.
*Appl. Phys. Lett.* **2012**, *100*, 094102.

(47) Duan, Z.; Pasquer, A. D.; Lu, Y.; Xu, Y.; Garfunkel, E. Effects of Mg composition on
open circuit voltage of $Cu_2O?Mg_xZn_{1?x}O$ heterojunction solar cells. *Sol. Energ. Mat.
Sol. Cells* **2012**, *96*, 292–297.

(48) Robertson, J.; Clark, S. J. Limits to doping in oxides. *Phys. Rev. B* **2011**, *83*, 075205.

(49) Knutsen, K. E.; Johansen, K. M.; Neuvonen, P. T.; Svensson, B. G.; Kuznetsov, A. Y. Diffusion and configuration of Li in ZnO. *J. Appl. Phys.* **2013**, *113*, 023702.